PHILOSOPHICAL TRANSACTIONS OF THE ROYAL SOCIETY A MATHEMATICAL, PHYSICAL & ENGINEERING SCIENCES

Variability in Atmospheric Circulation and Moisture Flux over the Arctic [and Discussion]

Mark C. Serreze, Roger G. Barry, Mark C. Rehder, John E. Walsh and D. Drewry

Phil. Trans. R. Soc. Lond. A 1995 **352**, 215-225
doi: 10.1098/rsta.1995.0065

Variability in atmospheric circulation and moisture flux over the Arctic

By Mark C. Serreze[1], Roger G. Barry[1], Mark C. Rehder[1] and John E. Walsh[2]

[1] *Cooperative Institute for Research in Environmental Sciences, Division of Cryospheric and Polar Processes, University of Colorado, Boulder CO 80309, USA*

[2] *Department of Atmospheric Sciences, University of Illinois, Urbana–Champaign, Urbana IL 61801, USA*

Mean characteristics and variability in the spatio-temporal distribution of Arctic water vapour and vapour fluxes are examined using several different rawinsonde-derived databases. Precipitable water averaged over the polar cap, 70–90° N, peaks in July at 14.0 mm. Large poleward fluxes near the prime meridian reflect transport associated with north Atlantic cyclones and, for most months, a local maximum in available water vapour. The mean vapour flux convergence averaged for the polar cap peaks in September. There is a mean annual excess of precipitation minus evaporation ($P - E$) of 163 mm, with a 78 mm range between extreme years. High $P - E$ is favoured by a meridional circulation accompanied by a more dominant North Atlantic cyclone track. No trend in annual $P - E$ is apparent over the 1974–1991 period.

1. Introduction

Uncertainties in the distribution of Arctic water vapour can cause errors in satellite-derived estimates of surface albedo (Rossow *et al.* 1989) and ice surface temperatures (Key & Haefliger 1992). Changes in water vapour flux convergence and precipitation minus evaporation ($P - E$) may alter river runoff into the Arctic Ocean, with consequent changes in the density structure of the upper ocean, possibly influencing sea ice production (Cattle 1985), and through ice advection, deep-water formation in the peripheral seas (Mysak *et al.* 1990). Although the Arctic response to anthropogenic greenhouse warming will likely be amplified due to the temperature–albedo feedback, an attendant increase in atmospheric moisture, through its added greenhouse effect, is expected to further enhance warming (Raval & Ramanathan 1989). Changes in the Arctic atmospheric moisture budget are also likely to be manifested by altered cloud cover, further impacting on the surface radiation budget. The characteristics of Arctic water vapour have been addressed as a component of global studies (e.g. Peixoto & Oort 1983; Gaffen *et al.* 1991; Peixoto & Oort 1992), for specific regions in the Arctic (e.g. Barry 1967), for means at 70° N (Serreze *et al.* 1994*a*) as well as for the entire Arctic Basin (Burova 1983; Burova & Voskresenskii 1976; Drozdov *et al.* 1976; Serreze *et al.* 1995*a*), but the need exists for a synthesis of the basic features of its variability. Here, we draw from some of our recent studies and summarize

Phil. Trans. R. Soc. Lond. A (1995) **352**, 215–225
Printed in Great Britain

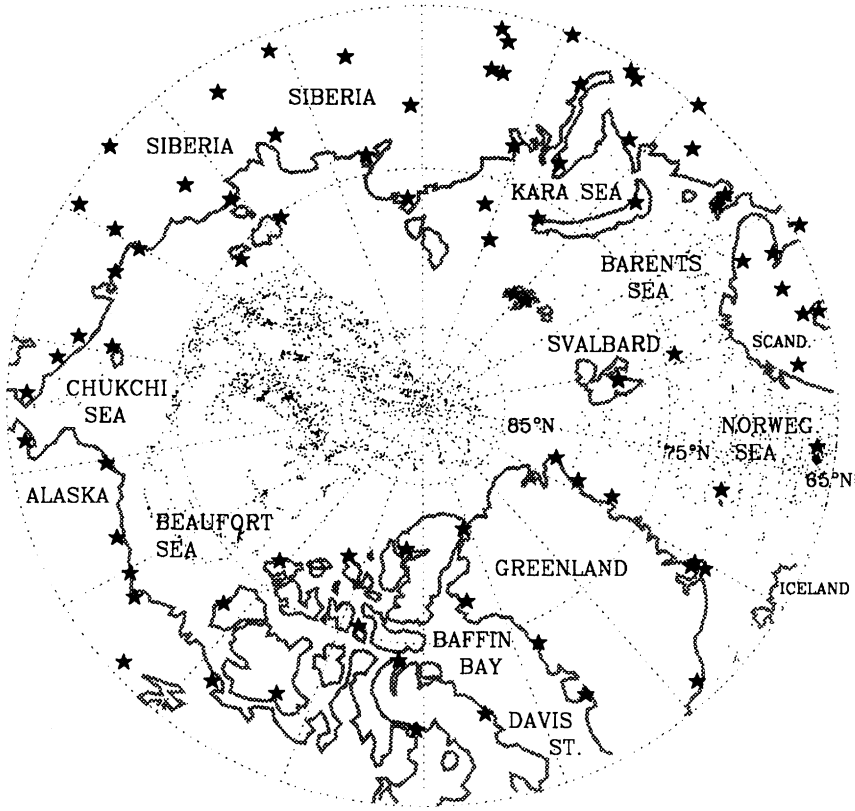

Figure 1. The distribution of fixed stations in the HARA during 1988 (stars) and drifting ice station and ship soundings (dots, plotted at every 10th sounding).

the characteristics of Arctic water vapour and its transports, using data from three rawinsonde archives.

2. Data and quality control

(*a*) *Rawinsonde archives*

The first dataset, the Historical Arctic Rawinsonde Archive (HARA) (Kahl *et al.* 1992), contains soundings taken one to four times per day for fixed stations north of 65° N. Records of at least 30 years are available for about 60 stations, typically extending through 1991. The second archive comprises soundings taken from 1–2 times daily from the Russian 'North Pole' (NP) series of drifting ice stations in the Arctic Ocean. The data coverage extends from 1954 through 1990, and includes records from NP 3–4, 6–17 19, 21–22, 26 and 28. While often only a single station was in operation at any one time, there are many periods with overlapping records from multiple stations. Some stations contain records of several years or more. Approximately 17 000 soundings are available. The third archive comprises approximately 16 500 soundings made from ships. These soundings, available from 1976–1991 at either 0000 or 1200 UTC, were primarily taken over the Norwegian and Barents seas (figure 1).

All soundings provide measurements of temperature, humidity and winds at both

fixed mandatory-reporting pressure levels (e.g. surface, 850 mbar, 700 mbar) and significant pressure levels (intermediate levels based on vertical-change criteria specified for the reporting of upper-air sounding data). Both data types are used here. The HARA and ship soundings typically extend up to at least 300 mbar. By contrast, the majority of the NP soundings extend only to about 700 mbar. We use all of the NP and ship data. As the number of soundings per station and number of significant levels reported were fewer prior to 1974 for many Eurasian stations in the HARA, we use HARA data for the 1974–1991 period only.

(*b*) *Quality control and processing*

All data were subject to extensive quality control procedures. These consist of a series of vertical consistency and limits checks discussed by Serreze *et al.* (1994*a*, *c*). Erroneous or questionable data values were discarded, and then refilled through vertical interpolation. The Canadian HARA station data often had missing surface winds. Consequently, missing surface winds in the HARA were obtained from a climatological relationship between surface and 850 mbar wind direction and wind speed, compiled from a five-year subset of all HARA soundings (Serreze *et al.* 1994*a*). Soundings over the Arctic Ocean rarely had missing surface winds; if one of these sounding had missing surface winds, it was simply discarded. Three summary datasets were then compiled. In the first dataset (D1), the 0000 and 1200 UTC HARA soundings for 1974–1991 were processed to obtain monthly station means of precipitable water (from the vertical integral of specific humidity) and vertically integrated vapour fluxes for five layers (surface–850 mbar, 850–700 mbar, 700–500 mbar, 500–400 mbar and 400–300 mbar). The station means were then passed into a Cressman (1959) interpolation procedure to provide data at 70° N at every 10° of longitude, allowing for analyses of the climatological transport 'pathways' of water vapour into and out of the Arctic, as well as estimates of climatological vapour flux convergence and precipitation minus evaporation ($P - E$) over the north polar cap (70–90° N). $P - E$ is estimated as (Alestalo 1983)

$$P - E = -\nabla \cdot \boldsymbol{F}_{\mathrm{m}} - \partial Q/\partial t, \tag{1}$$

where $-\nabla \cdot \boldsymbol{F}_{\mathrm{m}}$ is the horizontal convergence of the vertically integrated (surface to 300 mbar) meridional vapour flux ($\boldsymbol{F}_{\mathrm{m}}$) across 70° N, and $\partial Q/\partial t$ is the monthly change in precipitable water (Q) based on the means of all stations north of 70° N. The $\partial Q/\partial t$ term is typically 5–20% of the magnitude of the flux convergence, being largest in the transitional months (Serreze *et al.* 1994*a*). The flux convergence is

$$-\nabla \cdot \boldsymbol{F}_{\mathrm{m}} = \frac{1}{A} \oint \boldsymbol{F}_{\mathrm{m}} \, \mathrm{d}C, \tag{2}$$

where $\mathrm{d}C$ is the length along the 70° N circle (totalling 1.37×10^4 km) and A is the area enclosed (1.54×10^7 km^2). Interpolated fluxes, the flux convergence and $P - E$ were obtained for each month of each year, with the results for individual years then averaged. To be included in the analysis, a station for a given month and year had to have valid data for at least 75% of all possible days. For the second database (D2), monthly HARA station means not passing the 75% data-availability threshold were discarded, with new means then found via Cressman interpolation from surrounding stations. This resulted in a complete time series for all stations. Meridional fluxes, the flux convergence and $P - E$ over the north polar cap for each month and year were then determined by passing into the Cressman interpolation

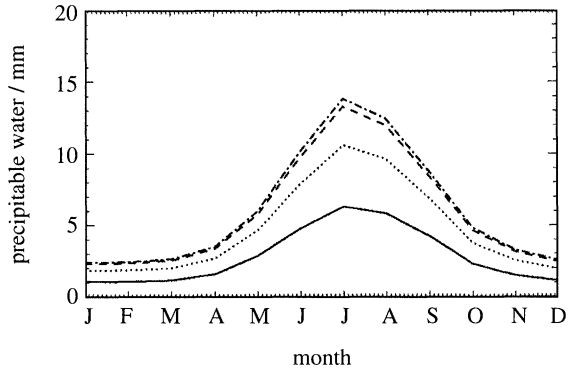

Figure 2. Mean monthly precipitable water (mm) averaged over the 70–90° N region for the surface–850 mbar (—), surface–700 mbar (···), surface–500 mbar (- - -) and surface–300 mbar (– · – · –) layers.

to 70° N only those station means requiring initial interpolation from surrounding stations for less than 30 of the possible 216 months in the 18-year data record. Long-term mean values are nearly identical to those derived from the D1 set. However, by minimizing the effects of changes in the station network, the technique provides for an internally consistent assessment of interannual variability in flux convergence and $P - E$. We have also compiled a gridded database (D3). Briefly, all ship and drifting station soundings were passed into the Cressman procedure to obtain climatological monthly means of precipitable water and vertically integrated vapour fluxes at NMC grid locations (Octagonal Grid Format) over the ocean. These grid-point means were then passed into a second interpolation that included long-term monthly means at the HARA stations, resulting in climatological monthly fields for all NMC grid locations north of 65° N. Details are provided by Serreze *et al.* (1994*b*, *c*). Elliot & Gaffen (1991) and Garand *et al.* (1992) discuss uncertainties in water vapour analyses at low temperatures and relative humidities and differences between countries in instrument types and reporting practices. Nevertheless, all of our analyses use the sounding data essentially as given. Since instrument changes and reporting practices have undergone frequent changes, and are often poorly documented, accounting for them fully would be impractical. Furthermore, as demonstrated in a series of sensitivity tests by Serreze *et al.* (1993*c*), these inhomogeneities may at worst result in potential errors of 5% in vertically integrated moisture variables (used here). This reflects the fact that problems in rawinsonde humidity data tend occur at the higher levels and lower temperatures at which water vapour is negligible.

3. Results

(*a*) *Precipitable water*

Figure 2 shows the seasonal cycle in precipitable water for 70–90° N from the surface–850 mbar, surface–700 mbar, surface–500 mbar and surface–300 mbar, based on the D3 dataset. Assuming that water vapour is negligible above 300 mbar, total precipitable water (surface–300 mbar) ranges by a factor of over five from about 2.5 mm in January to 14.0 mm in July, when surface and tropospheric temperatures are also highest. These values agree closely with those given by Peixoto & Oort (1992) based on an earlier dataset (1963–1973) with less vertical resolution. For all months,

PHILOSOPHICAL TRANSACTIONS OF THE ROYAL SOCIETY A MATHEMATICAL, PHYSICAL & ENGINEERING SCIENCES

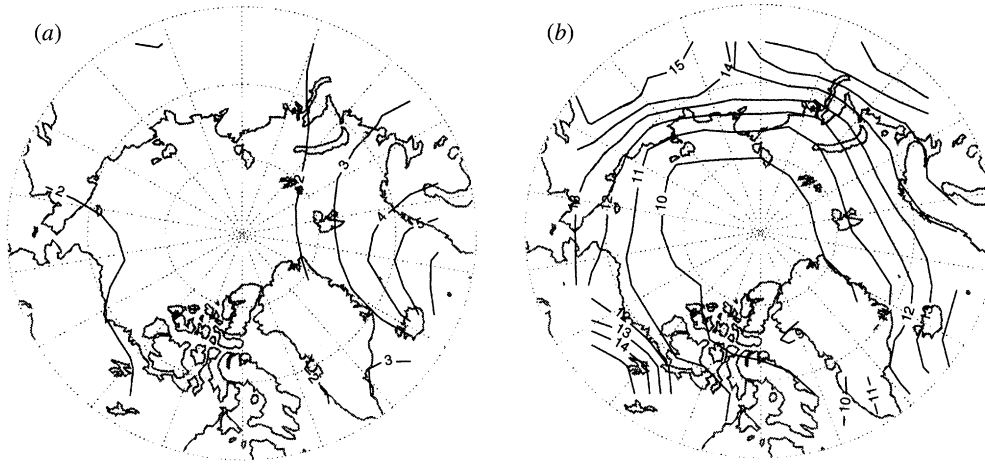

Figure 3. Mean precipitable water (mm) over the Arctic Basin in the surface–700 mbar layer for: (*a*) January, (*b*) July. Contours over the high (greater than 3000 m) Greenland ice cap have been omitted.

approximately 80% of precipitable water is found within the surface–700 mbar layer, and about 95% in the surface–500 mbar layer.

Figure 3 shows the spatial field of surface–700 mbar precipitable water for January and July from the D3 dataset. While gridded fields are available for the surface–300 mbar, fewer data points represent the ocean grid-point means above 700 mbar. For January (figure 3*a*), precipitable water increases from the central Arctic Ocean, Eurasia and Canada (less than 2 mm) towards the Atlantic side of the Arctic, peaking between Iceland and Scandinavia at 4–6 mm. This reflects the higher tropospheric temperatures in this region (Gorshkov 1983), allowing the atmosphere to hold more moisture. Qualitatively, the same pattern of precipitable water occurs from October through April. By contrast, the July pattern (figure 3*b*), qualitatively representative of May–September, is much more zonal, reflecting the more zonal temperature distribution.

(*b*) *Moisture flux*

Corresponding fields of the vertically integrated meridional vapour flux (surface–700 mbar) are provided in figure 4. For January (figure 4*a*), peak poleward transports are found between Iceland and Scandinavia (greater than 30 kg m^{-1} s^{-1}). This represents the combined effects of the regional maximum in available moisture and moisture transports associated with cyclonic activity along the primary North Atlantic storm track (Serreze *et al.* 1995*a*) (figure 5). A maximum in the poleward meridional flux in this region is observed for all months. The July fluxes are much larger (figure 4*b*); although the atmospheric circulation is weaker than in winter (Serreze *et al.* 1993), large fluxes are possible due to the greater availability of moisture. The pronounced area of negative (equatorward) fluxes over northern Canada in July (weakly present in January) relates to persistent equatorward winds on the eastern limb of the western North American longwave ridge. For all months, fluxes tend to peak in the lower troposphere, typically at about 850 mbar. This represents the 'trade-off' level between the effects of specific humidity decreasing with height, and winds increasing with height (Serreze *et al.* 1994*a*, *c*).

Figure 6 shows the longitudinal distribution of the vertically integrated (surface to

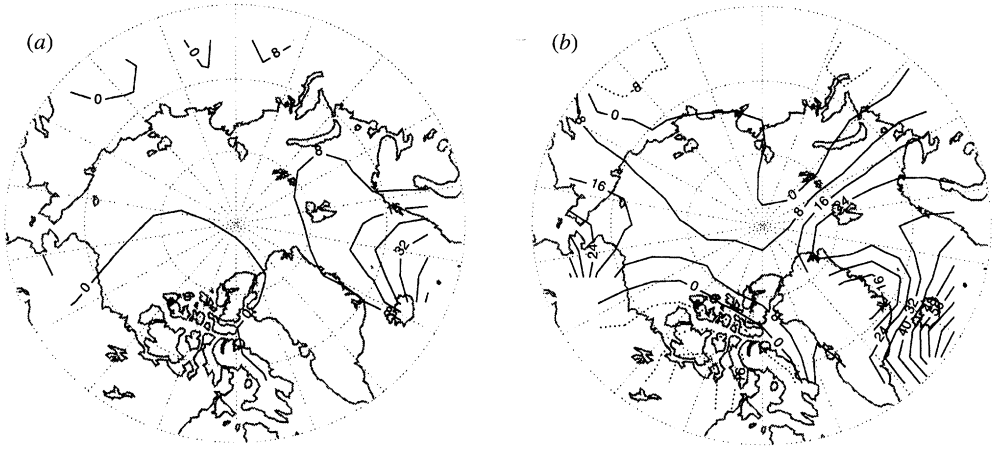

Figure 4. Mean vertically integrated meridional vapour flux (kg m^{-1} s^{-1}) over the Arctic Basin for the surface–700 mbar layer for (*a*) January and (*b*) July. Contours over the high (greater than 3000 m) Greenland ice cap have been omitted.

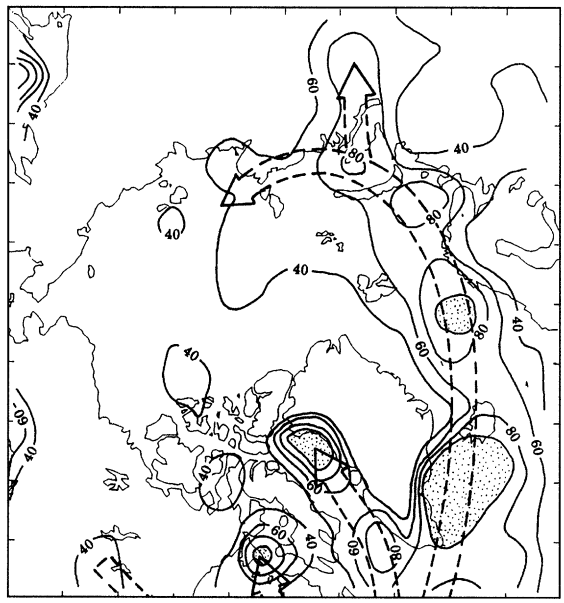

Figure 5. Counts of sea level cyclone centers at NMC grid point locations and generalized cyclone tracks for winter. Stipples denote areas with more than 100 cyclones (unpublished, based on the Serreze et al. (1993) cyclone detection algorithm).

300 mbar) meridional flux for January, July and September at 70° N, based on the D1 dataset. Each month shows peak poleward transports near the prime meridian and Baffin Bay, consistent with frequent cyclonic activity near these areas. A subsidiary peak is found near Alaska, best expressed in July and September. September also shows a fairly strong peak near 90° E. All months also show equatorward fluxes over the Canadian Arctic Archipelago.

PHILOSOPHICAL TRANSACTIONS OF THE ROYAL SOCIETY A MATHEMATICAL, PHYSICAL & ENGINEERING SCIENCES

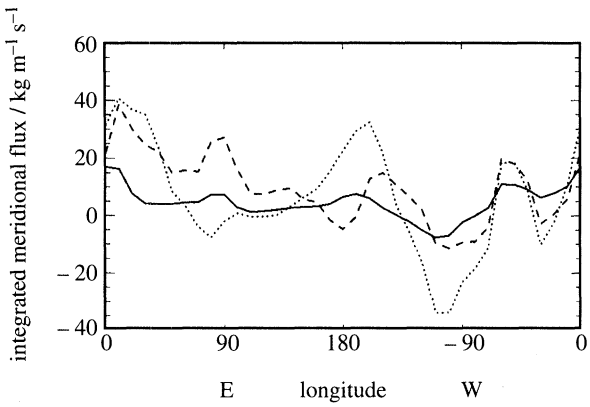

Figure 6. Longitudinal distribution of the mean (1974–1991) vertically integrated meridional water vapour flux (surface–300 mbar, in kg m^{-1} s^{-1}) at 70° N for January (—), July (· · ·) and September (- - -).

(*c*) *Moisture flux convergence*

The mean flux convergence into the polar cap is positive for all months. The monthly value, in terms of water depth averaged over the 70–90° N region, is about 10 mm for December through February, compared with 14 mm for July, and 22 mm in September, which represents the maximum for the year. As precipitable water is strongly decreasing in September (figure 2), $P - E$ also obtains its annual maximum of 26 mm in this month. The mean annual total $P - E$ of 163 mm is about 35% higher than that reported by Peixoto & Oort (1992), but compares closely with a value of 169 cm for the Arctic Ocean cited by Burova (1983). She also estimates that the contribution of precipitation from moisture evaporated and condensed which falls out within the region to be about 2/3 of the local evaporation (i.e. 120 mm) with a further contribution of 30 mm from condensation on the surface. Substituting into our $P - E$ value a climatological estimate of E for the 70–90° N region from the Korzun (1976) atlas (based on coastal and drifting station data), yields an areal-average annual precipitation of 266 mm, which compares favourably with the value of 293 cm for the same region from re-digitized precipitation values in the Gorshkov (1983) atlas. The reason why the flux convergence peaks in September, two months after peak precipitable water in July (figure 2), is apparent in figure 6. In July, the large poleward fluxes near the prime meridian, Alaska and over Baffin Bay are compensated by large moisture outflows over the Canadian Arctic Archipelago. By contrast, although the fluxes are generally more modest in September, there is less compensation between regions of inflow and outflow. Note in particular the poleward fluxes found from the Baffin Bay region eastward to about 140° E.

(*d*) *Time series of flux coverage and* $P - E$

Figure 7 provides the time series of the seasonal flux convergence expressed as liquid water averaged over the 70–90° N region for the period 1974–1991, based on the D2 dataset. For each year, the individual bar segments from bottom to top represent, respectively, the flux convergences for winter (January–March), spring (April–June), summer (July–September) and autumn (October–December). As over each annual cycle, $\partial Q/\partial t$ sums to zero, the sum of the seasonal flux convergences is annual $P - E$. The seasonal definitions used to compile figure 7 hence facilitate

PHILOSOPHICAL TRANSACTIONS OF THE ROYAL SOCIETY A MATHEMATICAL, PHYSICAL & ENGINEERING SCIENCES

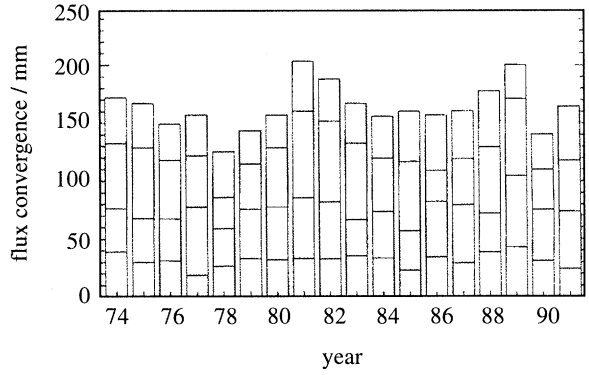

Figure 7. Time series of seasonal vapour flux convergence and annual $P - E$ (mm) averaged over the 70–90° N region, 1974–1991 (see text).

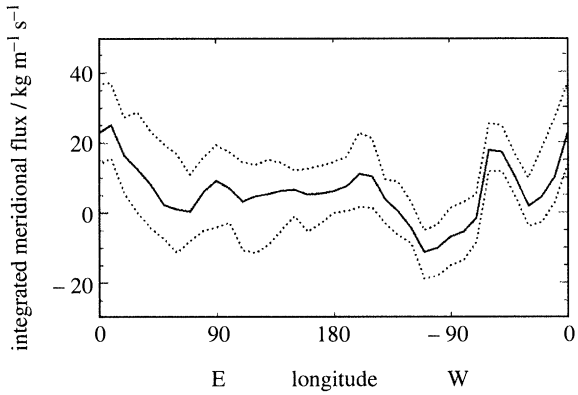

Figure 8. Longitudinal distribution of the mean annual vertically integrated meridional water vapour flux (1974–1991) and range between extreme years (surface–300 mbar, in kg m^{-1} s^{-1})

evaluation of seasonal contributions of the flux convergence to annual $P - E$ for standard calendar years. Annual $P - E$ ranges by 78 mm from a low of 125 mm in 1978 to a high of 203 mm in 1981. Although there is no apparent trend in $P - E$, there is some suggestion of a multi-year cycle, with higher values in the early to mid 1970s and early and late 1980s, which needs to be tested with a longer record. The mean seasonal flux convergences are 32, 44, 51 and 38 mm, respectively for winter, spring, summer and autumn.

(*e*) *Causes of variability*

Figure 8 shows the mean annual meridional flux by longitude at 70° N and the maximum and minimum at each longitude over the 1974–1991 period, based on the D2 dataset. The range between extreme years is highest (typically greater than 20 kg m^{-1} s^{-1}) from the prime meridian to 130° E and least around 60° W. A similar pattern is found for the seasonal flux values. This leads one to suspect that inter-annual variability in the seasonal flux convergence and annual $P - E$ are strongly controlled by flux variations over the Eurasian (0–130° E) sector. Composite analyses by Serreze *et al.* (1995*b*) of 500 mbar height, based on the three highest and lowest flux convergences for each season (not shown) reveal that large flux convergences

are favoured by a more meridional 'winter type' circulation, characterized by strong eastern North American and East Asian troughs. In turn, analyses of the distribution of sea level cyclone centers reveals a more pronounced North Atlantic cyclone track, with more cyclonic activity near the prime meridian and extending into the Kara Sea (winter, spring and autumn) promoting large vapour transports, or in summer, local increases over the Arctic Ocean accompanied by sharp reductions in cyclonic activity over Eurasia and Canada. Normally, summer cyclonic activity is frequent in these areas (Serreze *et al.* 1993). The low composites display essentially the opposite pattern. Variability in the strength of dominance of the North Atlantic cyclone track appears largely responsible for the large range in the meridional flux in the Eurasian sector, and hence variations in the flux convergence. Fluxes of liquid water, not considered here, would also be influenced by cyclonic activity.

4. Summary and conclusions

Using several rawinsonde archives, we have analyzed aspects of Arctic water vapour and its transports. For the 70–90° N region, surface–300 mbar precipitable water ranges from about 2.5 mm in January to 14.0 mm in July, with about 80% of the total column water vapour found in the surface to 700 mbar layer. During winter, peak values occur over the Atlantic side of the Arctic, reflecting the higher tropospheric temperatures, while during summer, a more zonal distribution is observed.

The meridional vapour flux exhibits large seasonal and spatial variability. Peak poleward transports found near the prime meridian manifest the greater availability of water vapour and moisture advection along the North Atlantic cyclone track. In turn, equatorward transports over the Canadian Arctic Archipelago reflect persistent northerly winds. These patterns are particularly apparent in the longitudinal distribution of the vertically integrated meridional flux across 70° N. The vapour flux convergence is positive for all months, peaking in September. The mean annual inflow into the Arctic corresponds to an excess of precipitation over evaporation of 163 mm. For the 1974–1991 period, $P - E$ ranges from a low of 125 mm in 1978, to a high of 203 mm in 1981, but no trends are apparent. Large seasonal flux convergences are favoured by a meridional 'winter type' circulation, characterized by a stronger or more dominant North Atlantic cyclone track.

This study was supported by NSF grants DPP-9214838 and DPP-9113673. The NSIDC staff is thanked for computer support.

References

Alestalo, M. 1983 The atmospheric water vapour budget over Europe. In *Variations in the global water budget* (ed. A. Street-Perrott, M. Beran & R. Ratcliffe), pp. 67–79. Dordrecht, The Netherlands: D. Riedel Publishing Co.

Barry, R. G. 1967 Variations in the content and flux of water vapour over north-eastern North America during two winter seasons. *Q. J. R. Met. Soc. Lond.* **93**, 535–543.

Burova, L. P. 1983 *Vlagooborot v atmosfere arktike* (Moisture exchange in the Arctic atmosphere), 128 pp. Leningrad: Gidrometeoizdat.

Burova, L. P. & Voskresenskii, A. I. 1976 Soderzhanie i perenos vlagi v atmosfere nad severnoi poliarnoi oblast'iu (Atmospheric moisture content and transport over the north polar area). *Leningrad, Arkticheskii i antarkticheskii nauchno-issledovatel'skii institut, Trudy* **323**, 25–39.

Cattle, H. 1985 Diverting Soviet rivers: some possible repercussions for the Arctic Ocean. *Polar Record* **22**, 485–498.

Cressman, G. P. 1959 An operational objective analysis system. *Mon. Wea. Rev.* **87**, 367–374.

Drozdov, O. A., Sorochan, O. G., Voskresenskii, A. I., Burova, L. P. & Kryshko, O. V. 1976 Kharakteriskiki vlagooborota v atmosfere nad skonami basseina severnogo ledovitogo okeana (Characteristics of the atmospheric water budget over Arctic Ocean drainage basins). *Leningrad, Arkticheskii i antarkticheskii nauchno-issledovatel'skii institut, Trudy* **327**, 15–34.

Elliot, W. P. & Gaffen, D. J. 1991 On the utility of radiosonde humidity archived for climate studies. *Bull. Am. meteor. Soc.* **72**, 1507–1520.

Gaffen, D. J., Barnett, T. P. & Elliot, W. P. 1991 Space and time scales of global tropospheric moisture. *J. Climate* **4**, 989–1008.

Garand, L., Grassotti, C., Halle J. & Klein, G. 1992 On differences in radiosonde humidity- reporting practices and their implications for numerical weather prediction and remote sensing. *Bull. Am. meteor. Soc.* **73**, 1417–1423.

Gorshkov, S. G. 1983 *World Ocean Atlas, Volume 3: Arctic Ocean* (in Russian), 184 pp. plus appendices. Oxford: Pergamon Press.

Kahl, J. D., Serreze, M. C., Shiotani, S., Skony, S. M. & Schnell, R. C. 1992 *In situ* meteorological sounding archives for Arctic studies. *Bull. Am. meteor. Soc.* **73**, 1824–1830.

Key, J. & Haefliger, M. 1992 Arctic ice surface temperature retrieval from AVHRR thermal channels. *J. Geophys. Res.* **97**, 5885–5893.

Korzun, V. I. 1976 *Atlas of world water balance,* 122 pp. Leningrad: Gidrometeiozdat.

Mysak, L. A., Manak, D. K. & Marsden, R. F. 1990 Sea ice anomalies observed in the Greenland and Labrador seas during 1901–1984 and their relation to an interdecadal Arctic climate cycle. *Climate Dynamics* **5**, 111–133.

Peixoto, J. P. & Oort, A. H. 1983 The atmospheric branch of the hydrological cycle and climate. In *Variations in the global water budget* (ed. A. Street-Perrott, M. Beran & R. Ratcliffe), pp. 5–65. Dordrecht, The Netherlands: D. Reidel Publishing Co.

Peixoto, J. P. & Oort, A. H. 1992 *Physics of climate*, 520 pp. New York: American Institute of Physics.

Raval, A. & Ramanathan, V. 1989 Observational determination of the greenhouse effect. *Nature, Lond.* **342**, 758–761.

Rossow, W. B., Brest, C. L. & Gardner, L. C. 1989 Global, seasonal surface variations from satellite radiance measurements. *J. Climate* **2**, 214–247.

Serreze, M. C., Box, J. E., Barry, R. G. & Walsh, J. E. 1993 Characteristics of Arctic synoptic activity, 1952–1989. *Meteor. atmos. Phys.* **51**, 147–164.

Serreze, M. C., Barry, R. G. & Walsh, J. E. 1994*a* Atmospheric water vapour characteristics at 70° N. *J. Climate* **8**, 719–731.

Serreze, M. C., Rehder, M. C., Barry, R. G. & Kahl, J. D. 1994*b* A climatological database of Arctic water vapor characteristics. *Polar Geog. Geol.* **18**, 63–75.

Serreze, M. C., Rehder, M. C., Barry, R. G., Kahl, J. D. & Zaitseva, N. A. 1995*a* The distribution and transport of atmospheric water vapor over the Arctic Ocean. *Int. J. Climatol.* (In the press.)

Serreze, M. C., Rehder, M. C., Barry, R. G., Walsh, J. E. & Robinson, D. A. 1995*b* Variations in aerologically-derived Arctic precipitation and snowfall. *Ann. Glaciol.* (In the press.)

Discussion

D. Drewry (*NERC, Polaris House, Swindon, UK*). Are the radiosonde data sufficient to examine regional scale questions such as trends in precipitation and consequential mass balance over the Greenland Ice Sheet?

R. G. Barry. In selected regions, the radiosonde network is adequate to compute the net moisture balance over a polygonal area. However, this approach is not recommended for small regions due to local anomalies in the wind components. Rasmusson

PHILOSOPHICAL TRANSACTIONS OF THE ROYAL SOCIETY A MATHEMATICAL, PHYSICAL & ENGINEERING SCIENCES

(1968) suggested that areas 2.0×10^6 km^2 or larger are required. Adequate temporal sampling of all synoptic weather events is equally critical.

The mass balance of the Greenland area (2.1×10^6 km^2) has in fact recently been examined using rawinsonde data by Robasky & Bromwich (1994). A decreasing trend of accumulation during 1963 to 1988 is indicated.

Walsh *et al.* (1994) similarly examine the moisture balance for the Mackenzie drainage basin (2.2×10^6 km^2 area).

Additional references

Rasmusson, E. M. 1968 Atmospheric water vapor transport and the water balance of North America. II. Large-scale water balance investigations. *Mon. Weather Rev.* **96**, 720–734.

Robasky, F. M. & Bromwich D. H. 1994 Greenland precipitation estimates from the atmospheric moisture budget. *Geophys. Res. Let.* **21**, 2495–2498.

Walsh, J. E., Zhou, X., Portis, D. & Serreze, M. C. 1994 Atmospheric contributions to hydrologic variations in the Arctic. *Atmos.-Ocean* **32**, 733–755.

PHILOSOPHICAL TRANSACTIONS OF THE ROYAL SOCIETY A MATHEMATICAL, PHYSICAL & ENGINEERING SCIENCES